sensors

MDPI

Article

A High Accuracy AC+DC Current Transducer for Calibration

Xia Xiao [1], Hongtian Song [1,2] and Hongbin Li [1,*]

[1] School of Electrical and Electronic Engineering, Huazhong University of Science & Technology, Wuhan 430070, China; xiaoxiahust@163.com (X.X.); songhtsky@163.com (H.S.)
[2] Southern Power Grid Research Institute Co., Ltd., Guangzhou 510663, China
[*] Correspondence: lihongbin@hust.edu.cn

Abstract: Facing a lack of high accuracy current standards in the calibration of AC (Alternating Current) + DC (Direct Current) measurement devices that function to measure DC and AC simultaneously, a measurement method with high accuracy is proposed based on zero-flux self-oscillating fluxgate. An iron core and two windings are added onto the single-iron-core double-winding structure of the traditional self-oscillating fluxgate. The added iron core and its upper winding are used to weaken the influence of ripple on the sensor's accuracy. The other one of the added windings is used for the feedback from the AC+DC magnetic potential, allowing the sensor to work in a zero-flux state and to measure AC+DC simultaneously. An AC+DC transducer prototype with an AC ranging from 0–500 A and DC 0–300 A is developed by selecting the core parameters and an optimized design of the circuit. The test results of the prototype show that the prototype can measure the AC and DC simultaneously, and the measurement accuracy reaches class 0.05 level in the nominal current range. This transducer can be used as a calibration standard of measurement devices for AC only, DC only, or AC and DC simultaneously. Compared with the AC+DC current transducer with the same accuracy level, the proposed transducer has fewer cores and simpler measuring circuit.

Keywords: self-oscillating fluxgate; zero-flux; AC+DC current transducer; calibration; standard CT (current transformer)

check for updates

Citation: Xiao, X.; Song, H.; Li, H. A High Accuracy AC+DC Current Transducer for Calibration. *Sensors* **2022**, *22*, 2214. https://doi.org/10.3390/s22062214

Academic Editor: Mario Luiso

Received: 17 February 2022
Accepted: 10 March 2022
Published: 12 March 2022

1. Introduction

DC in power grids is created due to induction from geomagnetic variations, DC power transmission, high-power electronic devices, and newly also by transformerless power inverters installed in solar power stations [1]. These currents, ranging in extreme cases up to hundreds of amperes, seriously affect the energy measurement and create a challenge in maintaining the DC-bias currents [2] at a certain level recommended by the grid codes [3]. This creates demand for the mixed AC+DC measurement, such as the DC-bias currents measurement [3] and AC measurement mixed with DC [4,5].

The standard CT used for the calibration of AC+DC measurement devices needs to have high AC and DC measurement accuracy under the condition of AC mixed with DC. The calibration of these AC+DC measurement devices require the input of AC mixed with DC. Due to the DC component, the accuracy of the standard CT based on the principle of electromagnetic induction will decline greatly and does not meet the requirements.

High-precision standard resistance is an ideal gauge of AC+DC, which is used as the calibration standard of anti-DC CT in Literature [6]. However, the high-precision standard resistance will consume power and heat up as the current increases.

Most of the reported high precision AC and DC measurement schemes are based on the magnetic modulation method. A precision DC/AC transformer is combined with a magnetic-modulation DC comparator and self-balancing AC comparator [7], which can measure AC and DC. The transformer consists of four iron cores and four windings. The electronic circuit includes an excitation oscillation circuit, peak detection circuit, amplifier circuit, and power amplification circuit. The errors at no DC component in the primary current are less than 20 ppm at currents between 1% and 100% of rated, and the errors, measured at DC between 10% and 100% of rated, are less than 100 ppm. There is no measurement data at AC mixed with DC. Meanwhile, the double core magnetic modulator has a false balance point, making its zero error larger.

Fluxgate magnetic modulation technology has the advantages of high resolution, wide measurement range, and high reliability. In the literature [8], a high-precision AC/DC proportional standard device based on the fluxgate and zero-flux principle was proposed. Two or four differential fluxgate sensors are symmetrically placed on the iron core to detect the residual magnetic potential caused by the imbalance between the primary and secondary currents. The accuracy of the prototype with a transformation ratio of 500:1 reaches level 0.01 at the power frequency AC 1–120% rated current and DC 1–120% rated current. Each fluxgate sensor requires external excitation. Additionally, to achieve the accuracy of level 0.01, the scheme requires four groups of fluxgate sensors to be symmetrically installed in the iron core to form a current sensor, which has high requirements for the processing technology of the iron core.

The magnetic modulator current sensing technology needs an external excitation source and a complex demodulation circuit. Meanwhile, the self-excited oscillation fluxgate sensor does not require an external excitation source, and its structure is simple. The operating principle of the open-loop self-oscillating fluxgate current sensor based on either the average current detection method [9,10] or the duty cycle method [11] has been studied. Compared with traditional fluxgate technology, the significant advantages of these sensors are their relatively simple modulation, demodulation circuits, and low cost.

However, due to the lower use of a magnetic core to compensate the modulation ripple induced in the primary and secondary windings due to the transformer effect, the obtained accuracy is only about 0.5% in the full scale of ±20 A [12,13].

A transducer combined with an improved self-oscillating fluxgate sensor with a magnetic integrator in a common feedback loop can measure DC up to ±600 A with a relative accuracy of 1.3 ppm in the full scale [14]. An iron core coil is added to the self-excited oscillation fluxgate sensor structure to weaken the conduction ripple in the iron core. The iron core coil and the self-excited oscillation fluxgate form a DC measurement channel. The third iron core detects the residual AC ripple in the iron core to further weaken the induced ripple in the iron core and form an AC measurement channel. In this paper, the researchers did not measure AC.

The main goal of this paper is to develop a standard current transducer for the calibration of AC+DC sensors with a simpler structure and sufficient accuracy. In this paper, a simpler AC+DC current transducer is proposed, which is composed of two iron cores and three windings. An iron core and two windings are added onto the single-iron-core double-winding structure of the traditional self-oscillating fluxgate. The added iron core and one of the windings are used to suppress the ripple in the iron cores. By matching core parameters and external circuit parameters, the ripple is suppressed to the greatest extent. In addition, through the LPF (low pass filter) and HPF (high pass filter) design in the electronic circuit, the self-excited oscillation fluxgate can measure AC and DC. The additional winding feeds back AC and DC to make the sensor cores work in a zero-flux state. In this way, the sensor only needs two iron cores and three windings to realize the high-precision simultaneous measurement of AC and DC.

The structure of this paper is as follows: the relevant existing works of AC/DC sensor, and fluxgate current sensor are reviewed in Section 1. Then, we introduce the single-core self-oscillating fluxgate current sensor principle in Section 2. In Section 3, the scheme for the AC+DC transducer is proposed in detail. In Section 4, the development of the AC+DC transducer is presented. We test the transducer to verify the accuracy and effectiveness of the scheme in Section 5. Finally, we summarize our work in Section 6.

2. Structure of Self-Oscillating Fluxgate Current Sensor

A schematic diagram of the open-loop self-oscillating fluxgate current sensor is shown in Figure 1. The operating principle of this circuit can be found in [9–11]. The excitation winding W_1 and the nonlinear core C_1 with high permeability and low magnetic saturation strength are equivalent to the nonlinear inductance L. The equivalent inductor L, the comparator A_1, the voltage dividing resistors R_1 and R_2, and the sampling resistance R_s constitute a self-oscillating circuit.

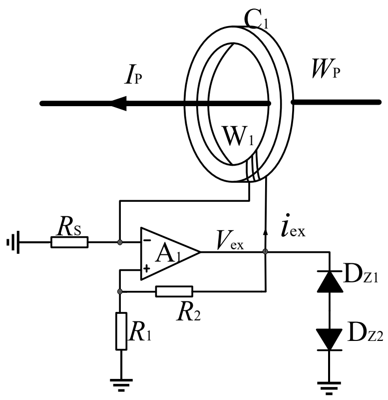

Figure 1. The self-oscillating fluxgate sensor circuit. C_1: iron core. W_1: excitation winding. W_p: primary winding. I_p: primary current. A_1: the comparator. R_1, R_2: the voltage dividing resistors. R_s: the sampling resistance. D_{Z1}, D_{Z2}: voltage limiting diode.

When the self-oscillating fluxgate sensor operates, the excitation voltage V_{ex} is a square wave signal with positive and negative symmetry. The iron core C_1 is in a state of alternating positive and negative saturation. Through piecewise linearization modeling on the excitation curve, it can be obtained that the period T of V_{ex} meets

$$\mathrm{T} = \frac{4N_1 B_S S}{V_{out}} \tag{1}$$

where N_1 is the number of turns of the excitation winding W_1. B_S is the magnetic saturation strength of the core C_1. S is the cross-sectional area of core C_1. V_{out} is the peak value of V_{ex}. Therefore, the excitation frequency of core C_1 can be calculated from the Formula (1).

According to the average current model [10], when the primary current is DC, during self-oscillating the average value i_{av} of excitation current i_{ex} meets

$$i_{av} = -\frac{N_P I_P}{N_1} \tag{2}$$

It can be seen from Formula (2) that the average excitation current i_{av} is proportional to the primary current I_P. Then the voltage generated by the exciting current i_{av} on the sampling resistance R_S can map the primary current I_P.

3. Principle of Zero-Flux Self-Oscillating AC+DC Transducer

3.1. Composition of AC+DC Transducer System

In this paper, a zero-flux AC+DC sensing scheme based on the structure of self-oscillating fluxgate is proposed. See Figure 2 for its system composition. The self-oscillating flux gate serves as the zero-flux detector to detect AC+DC unbalanced magnetic potential, and the AC+DC feedback current flows through the feedback winding W_F to make the cores in a zero-flux state. The ring core C_2, the exciting winding W_2, and the inverted amplifier A_2 reduces the electromagnetic induction noise, and the measuring accuracy is improved. The AC+DC sensing system is only of double-core three-winding configuration.

Therefore, the iron core structure of the transducer is simplified and the overall cost is reduced.

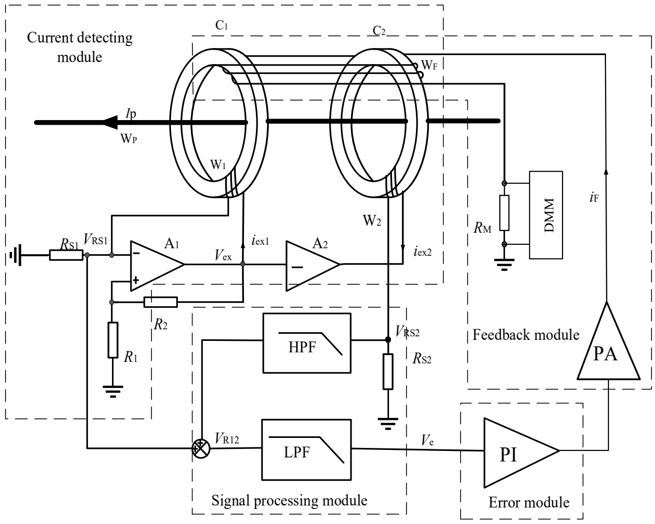

Figure 2. Composition of AC/C sensing system based on self-oscillating fluxgate principle. C_1, C_2: iron core. W_1, W_2: excitation winding. W_{F}: feedback winding. W_{p}: primary winding. I_{p}: primary current. A_1, A_2: the comparator. R_1, R_2: the voltage dividing resistors. R_{s1}, R_{s2}: the sampling resistance. R_{M}: the output sampling resistance. HPF: high pass filter. LPF: low pass filter. PI: proportional-integrator. PA: power amplifier.

In Figure 2, the sensing system includes the current detection module, signal processing module, error control module, and feedback module. In the current detection module, the ring iron cores C_1 and C_2 are nonlinear ferromagnetic materials of the same geometrical dimensions and magnetic parameters with high magnetic permeability, low coercive force, and high magnetic saturation induction strength. The excitation windings W_1 and W_2 with the number of turns N_1 and N_2 are evenly wound on the core C_1 and C_2, respectively. The comparator A_1, the winding W_1, and external resistances R_{S1}, R_1, and R_2 form a self-excited oscillation fluxgate. The square excitation voltage V_{ex} is output from A_1. The amplifier A_2 is an opposite single-proportional amplifier. The exciting currents of cores C_1 and C_2 are of the same amplitude and opposite phase, and, therefore, the cores C_1 and C_2 operates in an opposite exciting state.

When the primary current flowing in the primary winding W_P is I_P. The output voltage V_{RS1} and V_{RS2} on the resistor R_{S1} and R_{S2} is processed by the signal processing module, PI error module and PA circuit to generate feedback current in the feedback winding I_F. Finally, when the two iron cores are in zero flux state, the feedback current I_F is proportional to the primary current. The magnetic potential balance equation for the toroidal cores C_1 and C_2 satisfies

$$N_P I_P + N_F I_F = 0 \tag{3}$$

It follows from Formula (3) that when the sensing system reaches balance, the feedback current I_F is proportional to the primary current I_P, and the transformation ratio is N_F/N_P. The voltage signal V_{RM} output from the resistor R_M and primary current I_P shall satisfy the following requirements.

$$I_P = -\frac{N_F}{N_P} I_F = -\frac{N_F}{N_P}\frac{V_{RM}}{R_M} \tag{4}$$

The sensitivity S_{D1} can be derived from Equation (4):

$$S_{D1} = -\frac{dV_{RM}}{dI_P} = -\frac{N_P R_M}{N_F} \quad (5)$$

Equation (5) shows that the sensitivity of the AC+DC transducer is proportional to the resistance of R_M and inversely proportional to the number of turns N_F of feedback winding.

3.2. Improvement of Transducer Performance by Zero-Flux

Due to the transformer effect, the square wave excitation flux of C_1 will induce the ripple current in two windings W_1 and W_2, which affects the accuracy of the transducer. To suppress the noise generated by the electromagnetic induction, the ring iron core C_2, excitation winding W_2, and the inverse amplifier A_2 are used to improve the performance of the transducer.

If there is no core C_2 with anti-excitation and the transducer is of a single core structure, then the magnetic potential equation of the core C_1 is

$$N_P I_P + N_F I_F + N_1 i_{ex} = 0 \quad (6)$$

From (6), it is known that excitation current i_{ex} is still the main cause for the error of this transducer similar to traditional CTs.

Add a core C_2 with the same magnetic parameters and geometrical dimensions as C_1 and the excitation voltage V_{ex} of core C_1 is inverted and directly used as the excitation voltage of core C_2. Here, the magnetic potential equations of the cores C_1 and C_2 are, respectively:

$$N_P I_P + N_F I_F + N_1 i_{ex1} = 0 \quad (7)$$

$$N_P I_P + N_F I_F + N_2 i_{ex2} = 0 \quad (8)$$

Add (7) and (8) together, i.e., the cores C_1 and C_2 are considered a whole, for the following:

$$N_P I_P + N_F I_F = 0 \quad (9)$$

According to (9), the double-core self-oscillating fluxgate transducer can operate as a zero-flux state, thereby eliminating the impact on the measurement result of the single-core structure due to the electromagnetic induction, and achieving higher current detection accuracy of the AC+DC transducer.

3.3. Improvement of Transducer Performance by Demodulation Circuit Optimization

When the transducer measures the AC mixed with DC, the induced current on the excitation winding makes the excitation process of the iron core more complex and the nonlinear characteristics more obvious. A large number of high-frequency harmonics are generated in the excitation current. In this scheme, the high-frequency harmonic signals are effectively filtered out by the optimized demodulation circuit, and thus the measurement accuracy of the AC+DC transducer is improved.

When the primary current is the AC mixed with DC, the ring core C_1 is in the forward excitation state, and then the output voltage V_{RS1} on the sampling resistor R_{S1} consists of two parts: V_{L1} and V_{H1}. V_{L1} is a low-frequency signal, including a DC component V_{dc} proportional to the primary DC and an AC component V_{ac} proportional to the primary power frequency current. Meanwhile, a high harmonic current in the excitation signal also causes a high-frequency component V_{H1}. Since the magnetizing state of the toroidal core C_2 is precisely opposite to that of the core C_1, The output signal V_{Rs2} on the sampling resistance R_{s2} consists of V_{L2} and V_{H2} which are inverted with V_{L1} and V_{H1}, respectively. High-pass filtering is performed on V_{Rs2} and only the high-frequency component V_{H2} is retained. Thanks to the symmetry of the sensor structure and parameters, in theory, the two signals V_{H1} and V_{H2} have equal amplitudes and inverse phases. Then add V_{Rs1} and V_{H2} to get

$$V_{R12} = V_{Rs1} + V_{H2} = V_{L1} + V_{H1} + V_{H2} = V_{L1} \tag{10}$$

Equation (10) is an ideal output expression. However, the actual circuit cannot ensure consistency between C_1, C_2, and the additional circuit. It is impossible to eliminate the high-frequency component. It is necessary to filter the high-frequency component of the signal V_{R12} further by low-pass filtering, to reduce the influence of electromagnetic induction.

4. Development of AC+DC Transducer Prototype

4.1. Parameters of Cores

According to the requirements of a zero-flux self-oscillating flux transducer for the ferromagnetic parameters, the geometric and magnetic parameters of the cores C_1 and C_2 are summarized in Table 1.

Table 1. Geometrical and magnetic parameters of cores.

Parameters	Actual Meaning	Value	Unit
D_1	Outer diameter of core	85	mm
D_2	Inner diameter of core	75	mm
S_C	Core cross-section area	0.5	cm^2
L_e	Effective magnetic circuit length	25.12	cm
B_S	Saturated magnetic flux density	1.1	T
B_r	Residual magnetic flux density	0.66	T
H_c	Coercive force	0.6	A/m
μ_i	Initial relative magnetic permeability	200,000	-
μ_M	Maximum relative magnetic permeability	600,000	-

4.2. Circuit Parameter

(1) Comparator

The performance parameters, such as power supply, load capacity, noise, and bandwidth of comparator A_1, are factors that affect the measurement accuracy of the transducer. A high-precision operation amplifier OP27G with a dual power supply is used. The supply voltage is limited to ±15 V, and the output current can reach 40 mA under 100 ohm load. Meanwhile, OP27G is characterized by a wide frequency bandwidth and low noise. The input offset current is less than 35 nA, and the unity gain-bandwidth product is 8 MHz. The phase inverter A_2 and comparator A_1 is of the same type.

(2) Excitation Frequency

From Formula (1), the relationship between the excitation frequency f_{ex}, excitation voltage, and core parameters is as follows:

$$f_{ex} = \frac{V_{ex}}{4B_S N_1 S_C} \tag{11}$$

The excitation frequency f_{ex} should not be too high, since the vortex loss of magnetic material is proportional to the square of the excitation frequency f_{ex}. As the excitation frequency f_{ex} increases, the vortex loss in the core will increase, and the overall power consumption of the AC+DC transducer will increase. From (11), when the excitation voltage V_{ex} is constant, the higher the excitation frequency f_{ex}, the lower the number of turns N_1 of the excitation winding, and the higher the saturation current threshold of the core. Then, the core is difficult to enter the saturation area, which reduces the linearity of the transducer.

While the excitation frequency f_{ex} is too low, the number of turns N_1 of the excitation winding is too large, and the transducer's sensitivity will be decreased. Therefore, it is necessary to focus on the linearity and sensitivity in the design of parameters. According to the condition of the excitation frequency limit $f_{ex} > 2f$ (f is the frequency of primary current), when the detection bandwidth of AC and DC sensor is 0–50 Hz, the excitation frequency of the self-oscillating fluxgate transducer shall be designed to be higher than 100 Hz. In the design, the number of turns N_1 of the excitation windings W_1 is 175, and the excitation square wave voltage is ±5 V. From (11) and the core parameters in Table 1, the excitation frequency of the AC+DC transducer is calculated to be 129 Hz, meeting the requirements for bandwidth detection.

(3) LPF and HPF

The function of HPF is to retain the high-frequency signal in excitation winding W_2, its cut-off frequency is set to 59 Hz. The output signal of the HPF is added to the output signal of the excitation winding W_1 to weaken the mutual inductance effect. To further filter out the high-frequency signal in the synthetic signal, a low-pass filter retaining only DC and power frequency signals is set, and its cut-off frequency is also set to 59 Hz. Therefore, the high-frequency ripple signal generated by the mutual inductance effect is greatly attenuated in the output signal V_e.

(4) Feedback circuit

To reduce the output ripple of the power amplifier circuit, a traditional AB-type power amplification circuit is applied in this design. The power devices Q_1 and Q_2 are TIP 110 and TIP 117, which have the same parameters, and are high-power Darlington tubes, with the maximum AC output as high as 2 A. The power amplifier circuit is shown in Figure 3.

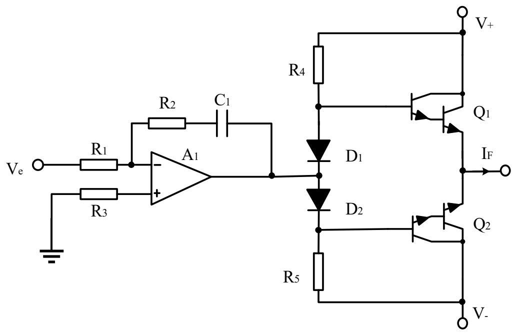

Figure 3. Schematic diagram of the power amplifier circuit.

4.3. Physical Transducer

Figure 4 shows the AC+DC transducer prototype based on the above principles and methods. Here are the main parameters of the given prototype. The transformation ratio: 1000:1; Rated AC: 500 A; Rated DC: 250 A; Sensitivity: 5 mV/A; and Bandwidth: 0–50 Hz.

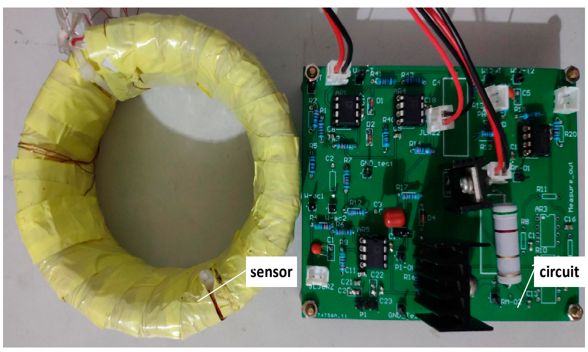

Figure 4. Prototype of zero-flux self-oscillating fluxgate AC+DC transducer.

5. Performance Test of AC+DC Transducer Prototype

The AC+DC measuring performance of the prototype is tested based on the proportional DC superposition method. See Figure 5 for the test principle and Figure 6 for the wiring diagram. The test equipment and parameters are as follows.

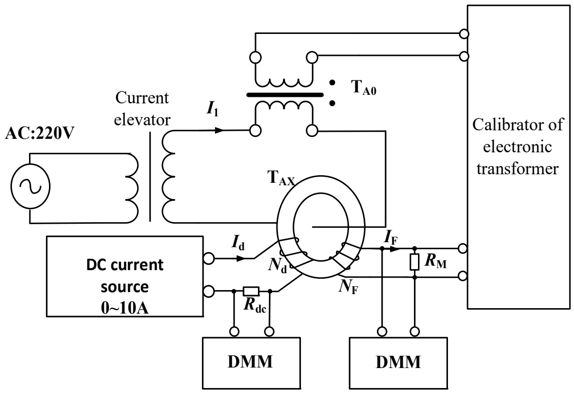

Figure 5. Schematic of error test based on proportional DC superposition method. T_{A0} : Standard current transformer. T_{AX}: the tested high-precision AC+DC transducer prototype. R_M: the output sampling resistance. N_d : winding turns of DC current.

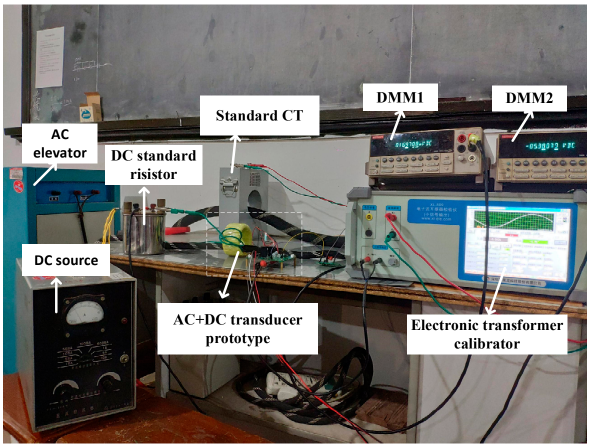

Figure 6. Photo of AC+DC transducer performance testing.

(1) Current elevator. Capacity: 20 kVA; Maximum output current: 3 kA;
(2) Standard current transformer T_{A0} Model: HL 28-5; Rated burden: 10 VA; Rated primary current: 500 A; Rated secondary current: 5 A; Accuracy class: 0.05;
(3) DC source. Model: YJ-10 A; Output current: 0;
(4) DC standard resistance R_{DC} Resistance: 0.1 Ω; Capacity: 10 A at 20 °C; Temperature drift: 10 ppm; Accuracy class: 0.01;
(5) Calibration instrument of electronic transformers. Model: XL-809; Input range: 0–8 V; Accuracy class: 0.05;
(6) Six and a half digital multimeter DDM. Model: KEITHLEY 2000; DC voltage accuracy: 0.002%.

In Figure 5, T_{AX} is the tested high-precision AC+DC transducer prototype. AC output by the elevator passes through T_{AX} and standard current transformer T_{A0}. DC is produced by the DC source and loaded on T_{AX} through equal ampere-turns. The output signal of T_{AX} is obtained from the sampling resistor R_M and input to the electronic transformer calibration instrument and DMM1 at the same time. The standard current transformer T_{A0} converts the primary AC into low voltage and transmits it to the electronic transformer calibration instrument. The electronic transformer calibrator gives the AC verification results through synchronous sampling and calculation. The DC standard resistance transforms the primary DC into low voltage and transmits it to DMM2. The verification results of DC are calculated through the synchronous readings of the two DMMs. The ratio error and phase error are, respectively, calculated according to the standard definitions of the transformer, respectively, expressed in percentage and minute.

By the Proportional DC Superposition Method testing scheme, AC measuring performance, DC measuring performance, and AC/DC mixed current measuring performance of prototype are explored.

5.1. AC measuring Performance Testing

According to the Verification Code for Current Transformer for Measurement, the DC circuit was disconnected during testing, and the ratio error and phase error of the AC+DC transducer prototype with forward and backward strokes of 5%, 20%, 100%, and 120% of the rated current were, respectively, tested. The test results are shown in Figure 7a,b.

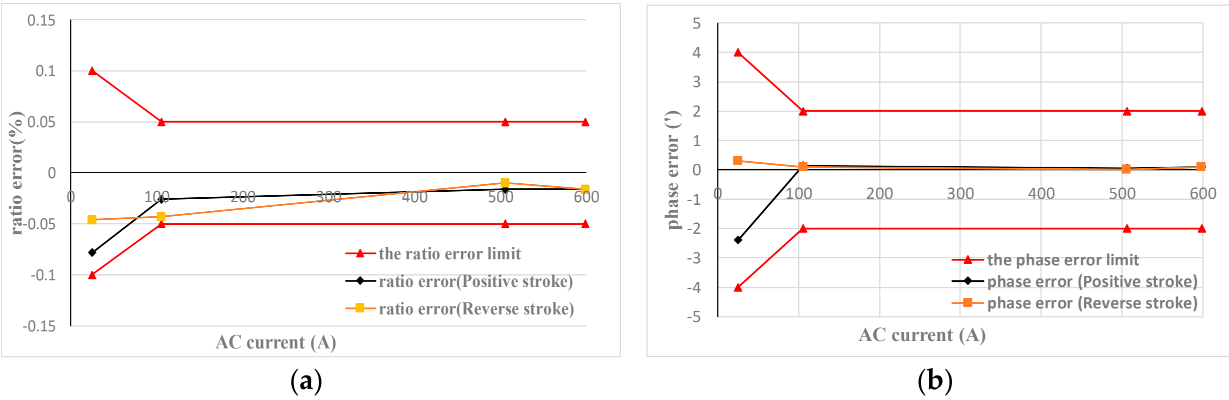

Figure 7. AC measuring performance test: (**a**) the ratio error for AC 0–600 A; and (**b**) the phase error for AC 0–600 A.

The red curve in Figure 7 is the limit curve of ratio error and phase error of the 0.05 class AC CT. It can be seen that the measured results of the prototype are within the error limits of the 0.05 class CT.

5.2. DC Measuring Performance Testing

Referring to the Verification Code for Current Transformer for Measurement for DC characteristics testing, the equal ampere-turn method is used to extend the DC measuring range and the primary AC circuit is disconnected during testing. The test results within the range of 0–120% rated DC are shown in Figure 8.

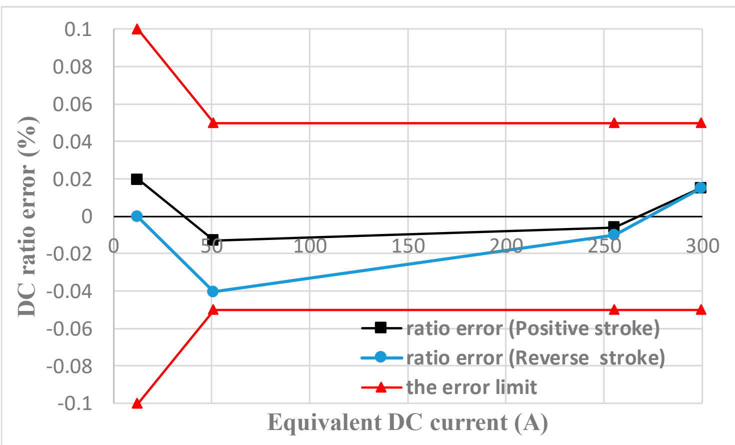

Figure 8. DC measuring performance test.

The horizontal coordinate of Figure 8 is the equivalent primary DC and the vertical coordinate is the scale error. The red curve is the limit curve of the 0.05 class DC CT proportional error. It can be seen that the DC scale error of the transducer is within the error limit of 0.05 class CT in the DC range of 0–300 A.

5.3. AC+DC Measurement Performance Testing

Along with the Proportion DC Superposition method and the equal ampere-turn method, AC and DC are input simultaneously to explore the measurement performance when AC and DC are applied simultaneously, including the effects of DC component on AC measurement and AC component on DC measurement.

5.3.1. Influence of DC Component on AC Measurement

The ratio error and phase error of the AC+DC transducer prototype within the range of 0–600 A are tested when the DC component is fixed at 20 A and 50 A respectively. The test results are shown in Figure 9.

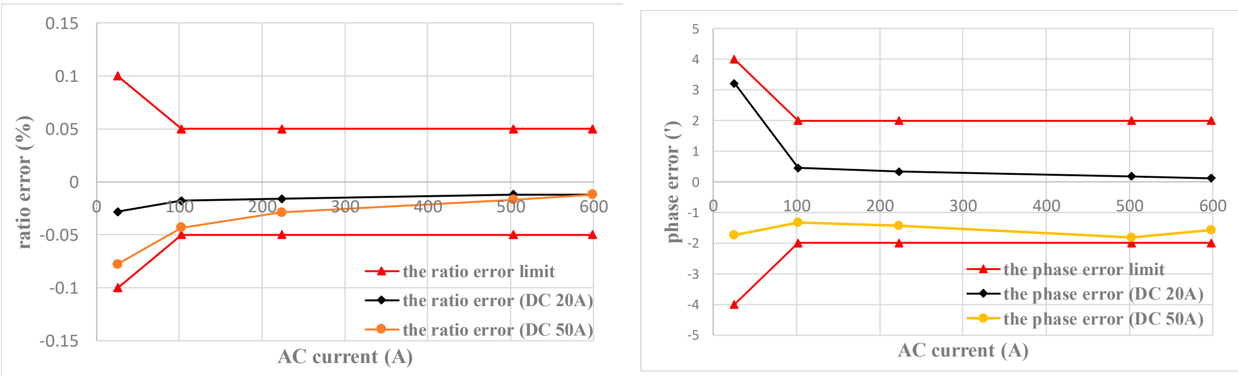

(**a**) (**b**)

Figure 9. Influence of DC on AC measurement: (**a**) the ratio error for AC 0–600 A; and (**b**) the phase error for AC 0–600 A.

The red curve in Figure 9 is the limit curve of ratio error and phase error of the 0.05-class AC CT. It can be seen from Figure 9 that with a fixed DC of 20 A and 50 A, the ratio error and phase error of the AC+DC transducer does not change significantly, and still satisfies the AC error limit of the 0.05-class. It indicates that the DC component has no significant effect on the measurement of AC.

5.3.2. Influence of AC on DC Measurement

The DC scale error within the range of 0–300 A is tested when the AC is fixed at 25 A and 250 A, respectively. The test results are shown in Figure 10.

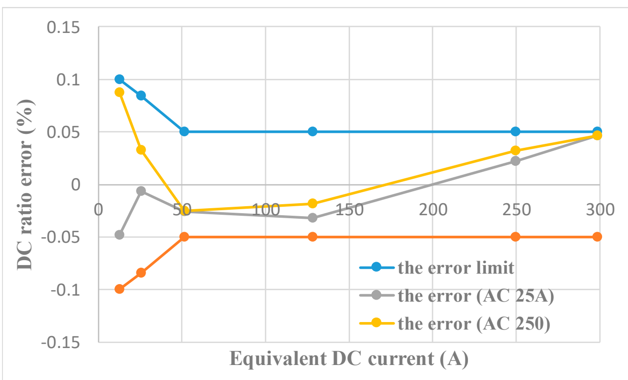

Figure 10. Influence of AC on DC measurement.

As shown in Figure 10, the red curve is the limit curve of the 0.05 class DC CT. It can be seen from Figure 10 that the DC measurement results still satisfy the 0.05 class DC error limit for an AC component of 25 A and 250 A. The magnitude of AC has no noticeable effect on the DC measurement error.

6. Conclusions

The measurement accuracy of the standard CT used for AC CT calibration cannot meet the calibration when AC and DC currents are mixed. It requires a high accuracy standard current transducer that can measure AC and DC simultaneously. An AC+DC transducer based on zero-flux self-oscillating fluxgate is proposed in this paper. Some parameters of the transducer are: Rated AC: 500 A; Rated DC: 250 A; Bandwidth: 0–50 Hz. The ratio error and phase error of the transducer prototype are within the error limit of class 0.05 CT at the range of 5–120% of the rated current When only DC or AC. The errors of the transducer are also tested at AC mixed with DC and DC mixed with AC. The ratio error and phase error of the prototype at the AC range of 0–600 A are within the error limit of class 0.05 CT when the DC component is fixed at 20 A and 50 A, respectively. The DC scale error at the range of 0–300 A is within the error limit of class 0.05 CT when the AC is fixed at 25 A and 250 A, respectively. The transducer can calibrate AC CTs, DC CTs, and anti-DC CTs with an accuracy level not high than 0.2.

The AC+DC transducer proposed in this paper has a simpler structure and only needs double cores and three windings. However, at present, the sensor has high accuracy only under the power frequency AC mixed with DC; that is, its bandwidth is limited. The research team is trying to expand the bandwidth of the sensor by changing the excitation frequency of the self-excited oscillation circuit and the matching of circuit parameters to make it more widely used, such as the calibration under half-wave current.

Author Contributions: Methodology, X.X. and H.L.; validation, X.X. and H.S.; investigation, X.X. and H.S.; resources, H.L.; data curation, H.S.; writing—original draft preparation, X.X.; writing—review and editing, X.X.; project administration, H.L.; funding acquisition, H.L. All authors have read and agreed to the published version of the manuscript.

Funding: This research received no external funding.

Institutional Review Board Statement: Not applicable.

Informed Consent Statement: Not applicable.

Data Availability Statement: The data used to support the findings of this study are available from the corresponding author, [X.X.] and [H.S.], upon request.

Conflicts of Interest: The authors declare no conflict of interest.

References

1. Gertmar, L.; Karlsson, P.; Samuelsson, O. On DC Injection to AC Grids from Distributed Generation. In *EPE 2005*; IEEE: Dresden, Germany, 2005; pp. 1–10, ISBN 90-75815-08-5.
2. Chang-yun, L.; Qingmin, L.; Huang, J.; Liu, H.; Zhang, L.; Siew, W.H. Research on the Temporary Performance of the Protective Current Transformers with DC Bias Excitation. In Proceedings of the UPEC Conference, Glasgow, UK, 1–4 September 2009.
3. Buticchi, G.; Lorenzani, E.; Franceschini, G. A DC Offset Current Compensation Strategy in Transformerless Grid-Connected Power Converters. *IEEE Trans. Power Deliv.* **2011**, *26*, 2743–2751. [CrossRef]
4. Jin, S.; Li, M.; Liu, J. Research on low anti-DC current transformer and its detection device. *Electr. Meas. Instrum.* **2016**, *53*, 59–64.
5. Han, T.; Jiang, T.; Liao, Y.; Wang, E.; Chen, J.; Yang, S. Simulation Investigation on Anti-DC Current Transformer with Double Core. In Proceedings of the 2021 IEEE 4th International Electrical and Energy Conference (CIEEC), Wuhan, China, 28–30 May 2021.
6. Wang, B.; Xiao, X.; Xu, Y.; Song, H. Research on test system of a novel anti-DC current transformer. *Power Syst. Prot. Control.* **2018**, *46*, 68–74.
7. So, E.; Ren, S.; Bennett, D.A. High-current high-precision openable-core AC and AC/DC current transformers. *Instrum. Meas. IEEE Trans.* **1993**, *42*, 571–576. [CrossRef]
8. Yue, C.; Xiang, Q.; Luo, X. Study on zero-flux AC/DC sensor based on fluxgate principle. *Electr. Meas. Instrum.* **2017**, *54*, 73–77.
9. Filanovsky, I.M.; Piskarev, V.A. Sensing and measurement of DC current using a transformer and RL-multivibrator. *IEEE Trans. Circuits Syst.* **1991**, *38*, 1366–1370. [CrossRef]

10. Ponjavic, M.M.; Duric, R.M. Nonlinear modeling of the self-oscillating fluxgate current sensor. *IEEE Sens. J.* **2007**, *7*, 1546–1553. [CrossRef]
11. Wang, N.; Zhang, Z.; Li, Z.; Zhang, Y.; He, Q.; Han, B.; Lu, Y. Self-oscillating fluxgate-based quasi-digital sensor for DC high-current measurement. *IEEE Trans. Instrum. Meas.* **2015**, *64*, 3555–3563. [CrossRef]
12. Velasco-Quesada, G.; Román-Lumbreras, M.; Conesa-Roca, A.; Jeréz, F. Design of a low-consumption fluxgate transducer for high current measurement applications. *IEEE Sens. J.* **2011**, *11*, 280–287. [CrossRef]
13. Yang, X.; Li, Y.; Guo, W.; Zheng, W.; Xie, C.; Yu, H. A new compact fluxgate current sensor for AC and DC application. *IEEE Trans. Magn.* **2014**, *50*, 4005704. [CrossRef]
14. Wang, N.; Zhang, Z.; Li, Z. Design and Characterization of a Low-Cost Self-Oscillating Fluxgate Transducer for Precision Measurement of High-Current. *IEEE Sens. J.* **2016**, *16*, 2971–2981. [CrossRef]